Indonesian Journal of Electrical Engineering and Informatics (IJEEI)
Vol. 10, No. 1, March 2022, pp. 60~71
ISSN: 2089-3272, DOI: 10.52549/ijeei.v10i1.3522

An Ensemble Classifier Based on Individual Features for Detecting Microaneurysms in Diabetic Retinopathy

Mohamed Jebran Pendekal[1], Shweta Gupta [2]

[1]Research Scholar, Faculty of Engineering and Technology, Jain University, Bangalore, India
[2]Associate Professor, Faculty of Engineering and Technology, Jain University, Bangalore, India

Article Info

Article history:

Received Nov 16, 2021
Revised Mar 6, 2022
Accepted Mar 11, 2022

Keyword:

Diabetic Retinopathy
Microaneurysms
Ensemble Classifier
Shape and intensity based features.
Gray Level Co-occurrence Matrix

ABSTRACT

Individuals with diabetes are more likely to develop Diabetic Retinopathy (DR), a chronic ailment that can lead to blindness if left undiagnosed. Microaneurysms (MA) are tiny red lesions that form on the retina in the early stages of Diabetic Retinopathy (DR). This paper investigates a unique approach for the automated early identification of microaneurysms in eye images. A unique ensemble classifier technique is suggested in this work. Classifiers like SVM, KNN, Decision Tree, and Naïve Bayes are chosen in this study for building an ensemble model. After preprocessing the image, certain common image characteristics such as shape and intensity features were retrieved from the candidate. The mean absolute difference of each feature is computed. Based on mean ranges that would give improved classification results, an expert classifier is chosen and trained. The outputs of the classifiers are integrated for each of the distinct characteristics, and the number of categories that have been most frequently repeated is utilized to reach a final decision. The process has been comprehensively validated using two available open datasets, like e-ophtha and DIARETDB1. On the e-ophtha and DIARETDB1, the ensemble model achieved an AUC of 0.928 and 0.873, sensitivity of 90.7% and 85%, specificity of 90% and 91% respectively.

Corresponding Author:

Mohamed Jebran Pendekal,
Department of Electronics and Communication Engineering,
HKBK College of Engineering, Bangalore, India
Email: jebranp@gmail.com

1. INTRODUCTION

Diabetes mellitus (DM) is a long-term illness that afflicts nearly all adults.The body cannot generate enough insulin or absorb it correctly, which causes type 2 diabetes. Elevated glucose levels throughout the body cause harm to nearly every internal organ. Diabetes is the most prevalent cause of damage to the feet, cardiovascular disease, and visual system. The phrase diabetic retinopathy refers to retinal damage resulting from diabetes. A worldwide survey found that in 2000 [1], the number of citizens with diabetes was 2.8%, and by 2030 this figure is predicted to rise to 4.4%. This projection shows that by the year 2030, the number of individuals who have diabetes will have increased in both developed and developing nations. DM development increases the likelihood of acquiring DR in the years to come.

Diabetic retinopathy is a side effect of diabetes that causes retinal blood vessels to be damaged. The clinical symptoms of retinopathy are caused by two fundamental pathophysiologic mechanisms: increased capillary permeability and also capillary closure [2]. It frequently affects both eyes and, if left untreated, can result in visual loss. Diabetic Retinopathy (DR), which has two distinctive variants: Non-Proliferative Diabetic Retinopathy (NPDR) and Proliferative Diabetic Retinopathy (PDR) [3]. In patients with NPDR, small retinal blood vessels are damaged somewhat, resulting in an accumulation of fluid, leakage, or rupture. The first is NPDR, which is followed by PDR, which is defined as a more advanced stage of the formation of new aberrant capillaries.

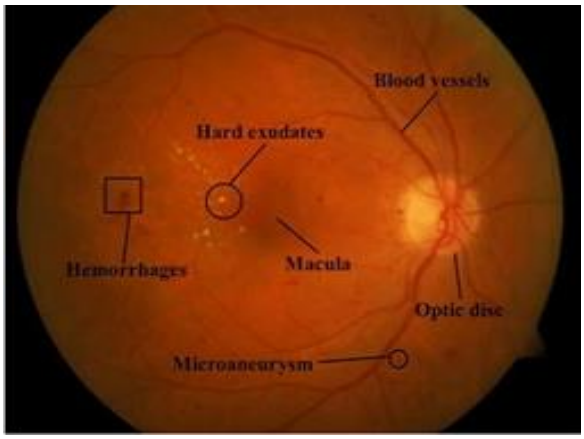

Figure 1. Lesions and other retinal characteristics

It is known that diabetic retinopathy is perceived by retinal vein enlargement. Additionally, tiny capillaries may experience pre-occlusive alterations. This leads to microaneurysms (MA), which are tiny bulges in the vascular walls. In addition to having vision issues, someone may be at risk of developing minimal non-proliferative diabetic retinopathy [4]. In fundus imaging, blood vessels, hemorrhages (HEM), and MAs all seem to be dark red, as shown in Figure 1. Microaneurysms are spherical deformations caused by the occlusion of blood or lipids in the retinal vasculature [5]. Red lesions, another name for microaneurysms, are an early stage of the disease that is essential to detect. At the onset of NPDR, only two or three red spots are visible. However, as the disease progresses, the number of lesions rises, as do the symptoms of HEM and bright lesions like Exudates(EX) and Cotton Wool Spots (CWS).

Fundus imaging mostly includes Digital fundus imaging (DFI), fundus fluorescein angiography (FFA), and optical coherence tomography (OCT) is currently used to clinically detect diabetic retinopathy (DR) [6]. The DFI imaging technique remains one of the recommended techniques for detecting DR since it is the most affordable. In the case of a large-scale screening programme, when ophthalmologists are engaged in just a small proportion of the overall programme, a computer-aided diagnosis (CAD) system can save both time and money.

An automated diagnosis system will therefore aid ophthalmologists in interpreting fundus images, eliminating flaws. Additionally, it can be used as a diagnostic tool by healthcare providers in areas where there is a shortage of qualified specialized doctors. It can help minimize patient waiting times, since the frequency of diabetic retinopathies is growing. Automated identification of these illnesses from retinal pictures is critical for elucidating the cause, diagnosing, treating, and planning surgery for retinal disorders.

The goal of supervised learning algorithms is to explore a hypothesis space in search of suitable hypothesis that will give outstanding predictions for a given instance. Finding a suitable hypothesis, even if the hypothesis space contains hypotheses that are well-suited for a specific situation, might be challenging. Ensembles integrate numerous hypotheses to generate a superior hypothesis. Ensemble learning is a method of constructing many base classifiers from which a new classifier is created that outperforms all constituent classifiers.

The existence of MAs is a warning indication that the disease process has begun. The objective of this research is to identify and locate lesions in the retina at the lesion level. The optimum characteristics based on shape and intensity were retrieved. An ensemble model comprising conventional machine learning classifiers was utilized. Rather than feeding all extracted features to individual classifiers of the ensemble model and then taking majority voting for classification, the proposed approach is based on a certain range of mean absolute difference for each feature. End-of-term class labelling will be decided by a majority vote.

Various medical disorders may be detected using machine learning techniques [7]. Despite the fact that there are a large number of studies on DR detection, only current literature on MA detection is used while compiling the literature on MA detection.

A three-stage approach is given by Shirbahadurkar et al. [8] to identify all the MAs in the fundus image of the retina. The first step utilizes morphological procedures and the Gabor filter to extract all potential candidates. Statistical, grayscale, and wavelet properties are used to build a feature vector for each candidate in the second stage. To categorize these possibilities, a feed-forward neural network (FFNN) and an SVM classifier are used. A vast number of feature sets were retrieved to distinguish MAs from non-MAs.

In [9] presented a technique for detecting early indications of DR, namely microaneurysms, by extracting Local Neighbourhood Differential Coherence Pattern (LNDCP) characteristics and employing an

ANN classifier. The pre-processing phase consists of a sequence of processes used to correct for luminance, contrast, and colour. During the segmentation step, the circular Hough transform is utilized to divide the optic disc. Classification is performed using the Feed Forward Neural Network (FFNN). This suggested technique is tested on ROC, which comprises of 50 images and a local dataset. In addition, a number of image preparation steps and optical disc segmentation are also done.

Long et al. [10] a technique for detecting microaneurysms utilizing machine learning methods such as Naive Bayesian, support vector machine, and K-nearest neighbour is presented for the early identification of DR. To begin with, an improved enhancement function generated from an investigation of Hessian matrix eigenvalues was used to enhance and segment blood vessels (BV). Shape characteristics and correlated component analysis were used to look for possible places for microaneurysm, not including blood vessels. After segmenting the image into patches, the characteristics of every microaneurysm candidate patch were retrieved and categorized as microaneurysm or non-microaneurysm.

To produce MA candidates, the method developed by Wu et al. [11] uses peak detection and region growth. During further identification of MA, the algorithm used KNN and obtained an FROC score of 0.273 on the e-ophtha MA repository. A localizing method by Wang et al. [12] used single spectrum analysis and a KNN classifier, but because there were extremely faint or indistinguishable, or blurry-outlined, MA, a few False Negatives (FN) were produced. The candidate extraction process failed to properly find certain relevant candidates.

MA detection approach is presented using directional intensity profiles by Lazar and Hajdu [13]. After locating the center peak of each cross-section profile, numerous statistical variables were retrieved and fed into a naive Bayes classifier. Dynamic shape features, referred to as shape features in [14], were utilized to help train a random forest classifier. However, missing lesions are associated with blood arteries, the results were False Negatives (FN).

Dynamic selection of the best combination of preprocessing stages and candidate extractors was utilized by Antal and Hajdu [15]. There were 25 possible combinations of five preprocessing procedures and five potential extraction strategies. Individual pairs were assessed for the best ensemble selection. Image preparation and candidate extraction stages are selected as an ensemble in this technique. A unique technique for MA identification in eye images was given in [16] by removing the Blood Vessels (BV) in the extraction phase and by utilizing a different kind of statistics, which were derived from geometric characteristics and an object rules-based classifier.

Numerous alternative techniques, such as unsupervised techniques, have been presented that do not involve the use of traditional classifiers. Mathematical morphology-based techniques are suggested to find microaneurysms in fundus pictures by Dharani et al. [17] and Joshi et al. [18].

The identification of MA via ANN and deep learning has recently gained popularity [19-21]. While CNNs have established themselves as strong tools for tackling a variety of computer vision applications, they do have several limitations. Learning these networks from scratch is difficult because of the time and resources required, including a significant quantity of annotated data and a GPU. They are also susceptible to overfitting and convergence issues.

Mathematical morphology-based approaches [11-12] and [17-18] tend to produce many false positives and skip the actual MAs when dealing with light changes. Furthermore, the outcomes of machine learning-based approaches show that strong manually designed features are required [13-14], yet feature design is a difficult task. The majority of the work on candidate classification utilized either traditional classifiers such as SVM, KNN, or Naive Bayes (NB) classifiers [11-12] or deep learning techniques [19-20]. Regardless of the available data, certain issues are simply too complex for a particular classifier to handle. More precisely, the decision boundary that divides data into various classes may be excessively complicated or beyond the space of functions. An ensemble of such linear classifiers may, however, be used to learn this non-linear boundary, provided they are combined in the right way so that the efficiency of the learning model can be improved.

The paper's primary contribution is a new ensemble classifier based on individual features for categorizing candidates as MAs or Non-MAs. This paper evaluated the effectiveness of the following classifiers: SVM, KNN, DT, and NB, each as a part of an ensemble, in their ability to correctly identify microaneurysms. The major contribution of this work is a unique ensemble classifier model based on individual characteristics for categorizing candidates as MAs or non-MAs. Simple image preprocessing, candidate extraction, and optimum feature extraction is performed to develop a reliable, automated Microaneurysm identification system. The suggested efficient technique introduces a unique approach to ensemble classification that is based on individual feature descriptors.

In the following paragraphs, you will find a breakdown of the structure of this article: Section 2 explains the approach for detecting microaneurysms that has been recommended. Performance ratings were presented in Section 3 in addition to the findings of the experiments. Finally, in Section 4, conclusions are drawn and recommendations for more research are given.

2. RESEARCH METHOD

2.1. Materials

The suggested system performance is evaluated using two of the most extensively used public databases, e-ophtha [22] and DIARETDB1 [23]. It is common practice to use these databases to discover vascular anomalies and diabetic retinopathy.

The database of e-ophtha is split into two sub-datasets: e-ophtha-MA and e-ophtha-EX, representing the existence of microaneurysms and exudates, respectively. e-ophtha-MA was used in this experiment, which consists of 148 colour fundus images with MAs or minor hemorrhages and 233 images without lesions in JPEG format. The images are 2544× 696 and 1440 ×960 pixels in size. Expert ophthalmologists have marked these images manually.

The DIARETDB1 dataset, abbreviated as DIAbetic RETinopathy DataBase-Calibration Level 1 (DIARETDB1), is another publicly accessible and frequently used dataset. This collection comprises 89 colour fundus images that have been saved in the PNG format and have a resolution of 1500 ×1152 pixels. 84 images include non-proliferative DR indications with signs of MAs, whereas five are normal.

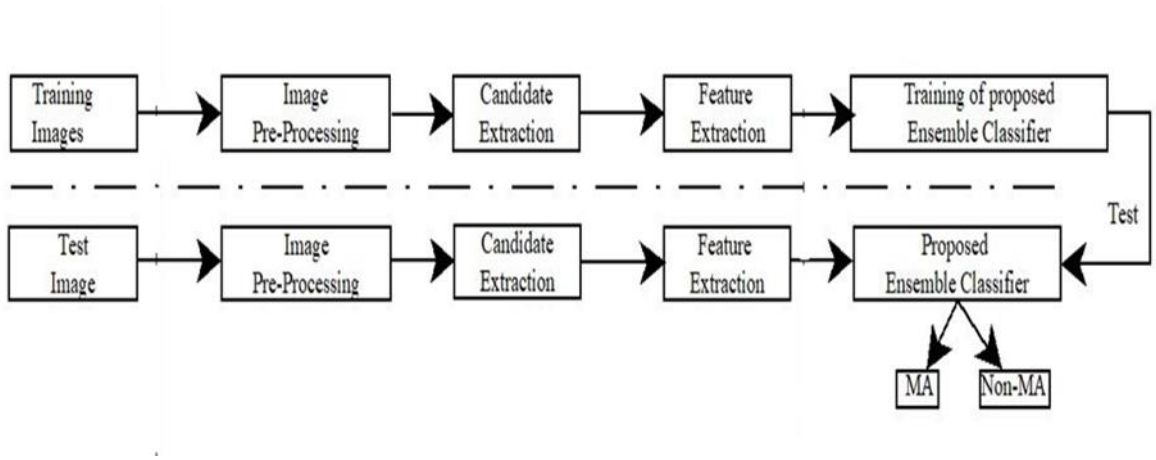

Figure 2. Proposed Microaneurysms detection system

2.2. Methods

The lesion classification processes for MA include image processing, extraction of candidates, feature extraction, and classification. To begin with, image preprocessing is done to enhance the overall image quality before candidate extraction and feature extraction. A Contrast Limited Adaptive Histogram Equalization (CLAHE) enhancement step is performed. The enrichment strategy effectively increases MA visibility while reducing noise. The early candidate pixels are retrieved via the use of morphological procedures. The candidates were analyzed for shape, intensity, and textural characteristics. A new approach to ensemble classification has been implemented, in which the mean absolute difference of each feature is determined. An expert classifier is selected and trained based on particular mean ranges that will produce superior classification results. The classifier outputs are embedded for all of the individual characteristics, and after determining the maximum number of occurrences of a label, the decisive conclusion will be reached. Figure 2 illustrates the proposed Microaneurysms detection system, and the following sub-sections detail the entire process.

2.2.1. Image Preprocessing

A preprocessing technique is used for a better contrast with the darker red areas. The green channel carries the most information in comparison to the other two channels, since it is capable of displaying a higher contrast between the targeted region and the background. As a result, the initial process in preprocessing would be to extract the image of the green channel, I_g. Next, a median filter [3 ×3] is used on the I_g image to generate the background image, I_{bg}. Figure 3 shows the stages of preprocessing.

Following that, the CLAHE [24] approach is used to balance the contrast with the surrounding background and make the important regions more noticeable. To decrease the influence of noise, even more, the enhanced image, I_{genh}, is generated by employing a Gaussian filter with a kernel size of [5 ×5].

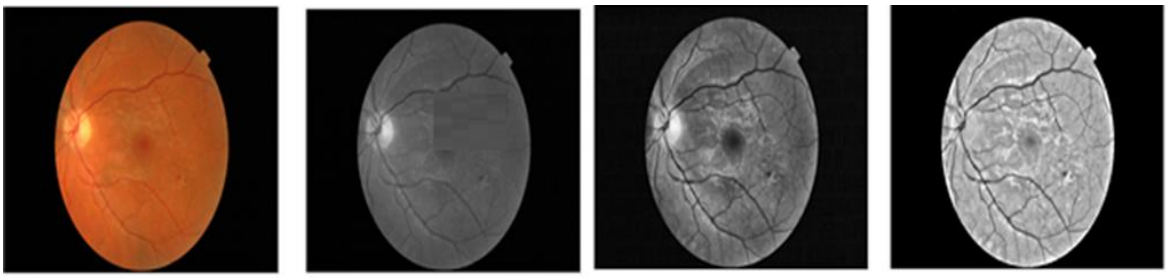

(i) (ii) (iii) (iv)

Figure 3. Processed image finding include: (i) the original image (ii) image in the green channel (iii) enhanced image in the green channel, and (iv) shade corrected image

The shade correction is described in equation (1) followed by normalization.

$$I_s = \frac{I_{genh}}{I_{bg}} \quad (1)$$

Where I_s represents the image after being corrected, I_{genh} the enhanced image, I_{bg} represents the background image approximated using a median filter with a kernel size of [68 ×68].

The last step is to divide I_s by its standard deviation, which results in a normalized global contrast image is expressed as

$$I_N = \frac{I_s}{\sigma(I_s)} \quad (2)$$

Where $\sigma(I_s)$ denotes the standard deviation of I_s **,** and I_N denotes the final preprocessed image.

2.2.2. Candidate Extraction

Figure 4. MA candidate detected for the image.

One of the objectives of this stage is to identify a preliminary collection of MA candidates, which are areas in which it is anticipated that MAs will exist. The aim is to minimize the number of non-MA identified items without losing any MAs that cannot be recovered later. The approach employed is based on Habib et al. [25]. To extract blood vessels, a linear structuring element is employed to conduct morphological closure on the preprocessed image in a variety of orientations. Subtraction of the preprocessed image from the top-hat filtered image follows. This method gets rid of the vessels while keeping the circular shapes that seem like MAs. After that, a Gaussian matching filter (σ = 1.0) is convoluted with the vessel-free image to highlight circular dark areas. Morphological closure is achieved using the disc as a structural element, which fills the

spaces inside the circular dark details that are MA candidates and are transformed into binary images. To improve the morphologies of the identified MA candidates, a region growing operation based on Fleming [26] is conducted and identified candidates are depicted in Figure 4.

2.2.3. Feature Extraction

To differentiate between true MA and false positives (FP), 11 characteristics were employed. Each candidate's features are extracted. These attributes are determined by the shape and intensity of MA candidates. The binary version of the image was used to calculate shape characteristics, while the grayscale version was used to compute intensity features. The retinal image's texture is analyzed directly using the GLCM [27-28]. Second-order statistical texture features are computed using GLCM. Utilizing GLCM, energy and homogeneity are computed. Table 1 includes a list of the retrieved features.

Table 1. Extracted candidate attributes

Shape-based features:		
a1	Area(A):	The number of pixels that make up the MA candidate area on its whole.
a2	Perimeter:	The periphery is the candidate circumference.
a3	Eccentricity:	A measure of the distance between the foci of the ellipse (d_foci) to the length of its main axis (l_main). Eccentricity measures how different something is from a circle. $(\varepsilon = \frac{d\_foci}{l\_main})$
a4	Extent:	It is obtained by taking the area of MA candidates (A) and dividing it by the entire bounding box area (A_{bb}). $(E = \frac{A}{A_{bb}})$
a5	Aspect Ratio:	The length ratio of the chosen region's major axis to minor axis.
a6	Orientation:	The angle formed by the x-axis and the primary axis of the ellipse.
Intensity based features:		
a7	Max Intensity:	The Intensity of the pixel has the highest value in the MA candidate area.
a8	Average Intensity:	Intensity levels in the MA candidate region averaged as a whole.
a9	Min Intensity:	The pixel with the least intensity in the MA candidate region.
GLCM features:		
a10	Energy:	It reflects the candidates grey distribution and texture thickness homogeneity. $Energy = \sum_{i,j=0}^{N-1}(P_{i,j})^2$ where $P_{i,j}$ −The normalised symmetrical GLCM element i,j, on the GLCM texture page of variable properties dialogue box under quantization, the number of grey levels in the picture is set as N.
a11	Homogeneity:	In GLCM, this measures how closely the components are distributed along the diagonal. $(Homogeneity = \sum_{i,j=0}^{N-1} \frac{P_{i,j}}{1+(i-j)^2})$

2.2.4. Classification

Ensemble systems employ a technique of creating several classifiers and combining their outputs in such a way that the combined performance outperforms that of a single classifier. These systems typically employ two paradigms: classifier selection and classifier fusion [29]. Every classifier has expertise in a subset of the whole feature space as part of classifier selection. The classifier combination is based on the given feature vector. Finally, the decision may be made by using a single classifier. Classifier fusion differs in that it first trains all classifiers in the whole feature space, instead of only some of them. Classifier outputs are commonly standardised to the [0, 1] interval, and these values are used to ascertain the degree to which each class has been supported by the classifier. To construct an ensemble, use algebraic rules like majority voting, maximum/minimum, sum/product, or other posterior probability combinations.

The suggested ensemble classifier combines selection and fusion. Algorithm 1 summarizes the suggested categorization approach. An expert classifier is chosen and trained based on individual features.

Algorithm1:Proposed Ensemble Classifier

Input- Input image I
Output- MA/Non-MA label for each lesion candidates.
$I_p \leftarrow$ Image preprocessing (I), carry out the fundamental image preparation steps outlined in equations (1) and (2).

lesion_cand(n) ← segmentation (I_p),perform candidate extraction.

for all lesion candidates:
  Feature_vector←compute shape, intensity and GLCM based features extraction to be done.
end
for each of the selected feature:
  Obtain the mean absolute difference $M_{1,j}$ obtained by equation (7)
  If $M_{1,j} < \theta_1$:
    E ← call the SVM model, train the SVM model for k-fold until accuracy > 60%, and receive the classification C =0 or 1 for Non-MA or MA, add C to the ensemble (E).
  If $\theta_1 < M_{1,j} < \theta_2$:
    E ← call KNN model, train the KNN model for k-fold until accuracy > 60%, and receive the classification C =0 or 1 for Non-MA or MA, add C to the ensemble (E).
  If $\theta_2 < M_{1,j} < \theta_3$:
    E ← call the NB model, train the NB model for k-fold until accuracy > 60%, and receive the classification C =0 or 1 for Non-MA or MA, add C to the ensemble (E).
  If $M_{1,j} > \theta_4$:
    E ← call the DT model, train the DT model for k-fold until accuracy > 60% and receive the classification C =0 or 1 for Non-MA or MA, add C to the ensemble (E).
end
Evaluate the ensemble, E, decide the final class label with maximum repeated label (C) by using majority voting technique which gives the final result of test candidate under test.

Let F be the feature vector table obtained by extracting the features from the MA and non-MA candidates as described in equation (3).

$$F = \begin{bmatrix} x_{1,1}\, x_{1,2}\; x_{1,3} & & x_{1,11} \\ x_{2,1}\, x_{2,2}\, x_{2,13} & & x_{2,11} \\ x_{m,1} x_{m,2} x_{m,13} & & x_{m,11} \\ y_{1,1} y_{1,2}\, y_{1,3} & \cdots & y_{1,11} \\ y_{2,1} y_{2,2}\, y_{2,3} & & y_{2,11} \\ y_{n,1} y_{n,2} y_{n,13} & & y_{m,11} \end{bmatrix} \quad (3)$$

Where $\{x_{1,1}, x_{1,2}, x_{1,3}, \ldots x_{1,11}\}$ represent the feature values for one candidate's MA class and similarly $\{y_{1,1}, y_{1,2}, y_{1,3}, \ldots y_{1,11}\}$ represent the feature vectors for one candidate's Non-MA class. Equal consideration will be given to both MA and non-MA candidates to avoid the problem of data imbalance in machine learning. Let N denote the total number of MA and non-MA candidates.

Let us represent two sub-feature matrices of MA and non-MA candidates as $f_1 = F(1{:}N/2, k)$ and $f_2 = F(\frac{N}{2} + 1{:}N, k)$ where k represents the number of feature columns in this case k=11.

The following equations are used to determine the mean absolute difference for the first column feature:

$$l_1 i, 1 = \frac{f_1 i, 1 - mean(f_1 i, 1)}{std(f_1 i, 1)} \quad (4)$$

$$l_2 i, 1 = \frac{f_2 i, 1 - mean(f_2 i, 1)}{std(f_2 i, 1)} \quad (5)$$

$$di, 1 = abs(l_1 i, 1 - l_2 i, 1) \quad (6)$$

$$M_{1,j} = mean(di, 1) \quad (7)$$

Where $l_1 i, 1$ indicates the matrix feature vector values for the MA class's first column feature, where i=1,2…. N/2 rows of total number of candidates, $l_2 i, 1$ represents the matrix feature vector values for first column feature of Non-MA class, $mean(f_1 i, 1)$ is the mean of the MA class's first column feature. Similarly, standard deviation is represented as $std(f_1 i, 1)$. The difference feature vector is represented by $di, 1$, $M_{1,j}$ denotes the absolute difference with j=1, i.e. the first feature column. j=1, 2...11 column characteristics.

As stated in equations (3) to (7), the value of $M_{1,j}$ mean absolute difference is determined for each column feature in the feature set table. After conducting extensive iterations, it is discovered that if the features have an $M_{1,j}$ value inside a specified range, a particular classifier will perform better. It is as follows:

If $M_{1,j} < \theta_1$, θ_1 is the threshold range θ_1 =0.96, the SVM classifier [30] is employed. It attempts to discover a hyperplane with the greatest margin by finding the closest points on that plane. If 0.96<M<θ_2 where θ_2 =1.15 is the range, the KNN Classifier [11-12] method finds the distance between these locations. The Euclidean distance is the most frequent method. Naïve Bayes Classifier [31]is implemented if θ_2<M<θ_3 where θ_3 =1.4 is the threshold range. The Bayes Theorem influenced the Naive Bayes Classifier. The most often used approach is to choose the most likely hypothesis; this is referred to as the maximal a posteriori or MAP decision rule. The objective of Naive Bayes is to maximize the probability of selecting class y. M>θ_4 , wehre θ_4 =1.5, a decision tree (DT) is a hierarchical architecture with nodes and branches that is deployed. The tree's construction uses information gained to decide which features to split. Entropy refers to the quantity of data required to correctly characterize a sample. Then make a decision on the final class label that has the highest number of repeated labels and provides the final result of the test characteristics under examination.

3. RESULTS AND DISCUSSION

E-ophtha-Ex dataset is excluded because our emphasis is on MA identification. The E-ophtha-MA database contains 148 images with MA and 233 images without MA. In the E-ophtha-MA dataset, ninety-eight images of MA were utilized for training with 10-fold cross validation, while the remaining 50 images were used for testing, following the general thumb rule of 70% images for training and remaining 30% for testing. To avoid data imbalance, an equal number of MA and non-MA candidates were extracted from the MA and normal images. Similarly, with the DIARETDB1 data set, 59 images are used for learning with 10-fold cross validation, and 30 images are used for testing

The classifier was trained on each image in the training set using the aforementioned attributes. Using a trained classifier, each test image was examined to determine if the candidate was MA. The results of MA identification were assessed at the lesion level using NB, KNN, SVM, Decision Tree, and suggested Ensemble classifiers.

The receiver operating characteristic (ROC) plot, which is sometimes referred to as the ROC curve, plots the sensitivity (SEN) and 1-specificity (SPE) (false positive rate, FPR). The region beneath this curve is known as the AUC. As the value approaches unity, the classifiers predictive accuracy improves. The two variables were computed in the following manner:

$$FPR = 1 - SPE = 1 - \frac{TN}{TN + FP} \tag{8}$$

$$SEN = True\ Positve\ Rate = \frac{TP}{TP + FN} \tag{9}$$

Where True Positive (TP) shows that MA has been accurately estimated, the significance of True Negative (TN) implies that non-MA has been accurately anticipated. The False Positive (FP) shows that non-MA is being projected as MA when it is not. Furthermore, False Negative (FN) implies that MA has been incorrectly anticipated as non-MA.

On two databases, the suggested ensemble model has the maximum area under the curve of 0.928 and 0.873, respectively, according to the ROC plot as shown in Figure 5 and Figure 6. When the same set of features is fed to each classifier individually, the individual classifier's performance suffers. The ROC plot shows how accurate it is to separate real MAs from non-MAs. The ROC curve demonstrates a TPR/FPR trade-off. The AUC indicates how well the model predicts the likelihood of a class YES over a class NO. In Figure 5, the suggested ensemble classifier has an AUC of 0.928 and the KNN classifier has the least performance of 0.823 when all features are directly supplied to the classifier. In Figure 6, the suggested ensemble classifier has an AUC of 0.873 and once again the KNN classifier has low AUC of 0.763. When all of the extracted features were supplied to the individual classifier, the SVM classifier beat the KNN, NB, and DT classifiers, with AUCs of 0.871 and 0.849 for the e-ophtha and DIARETDB1 datasets, respectively.

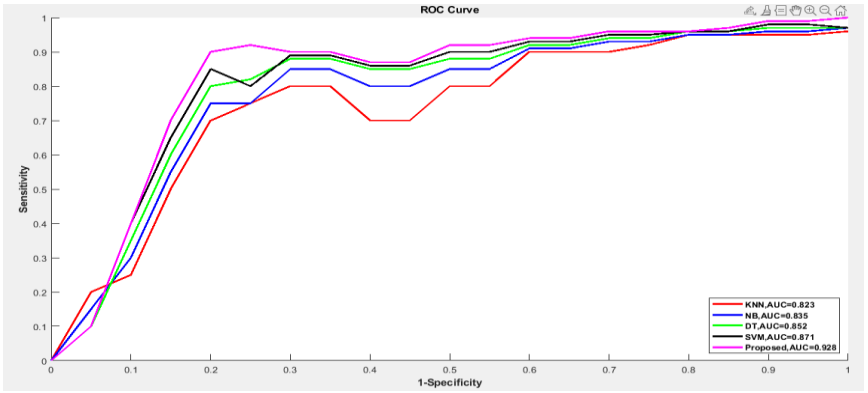

Figure 5. ROC curves of proposed and individual classifiers for E-ophtha MA dataset

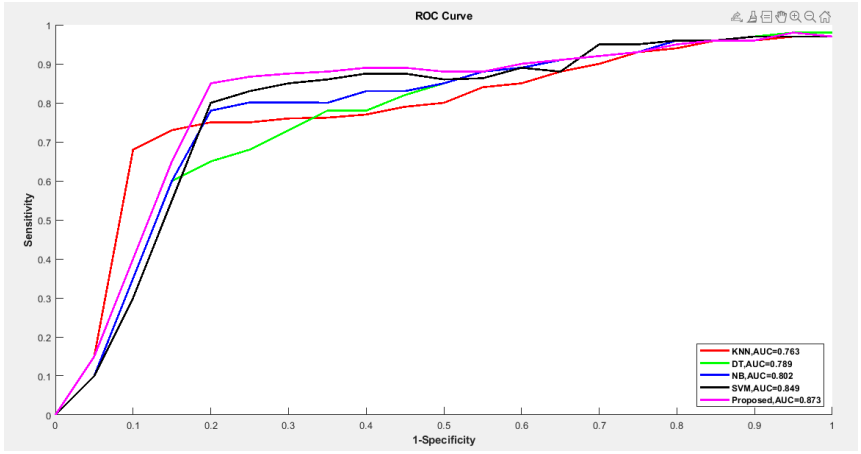

Figure 6.ROC curves of propose and individual classifier for DIARETDB1 dataset

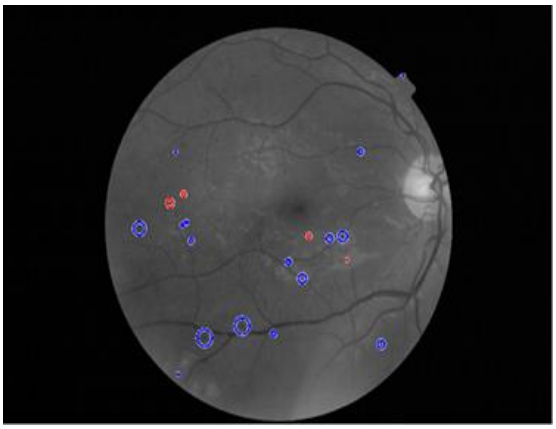

Figure 7. lesion level assessment (DS000DPJ image)

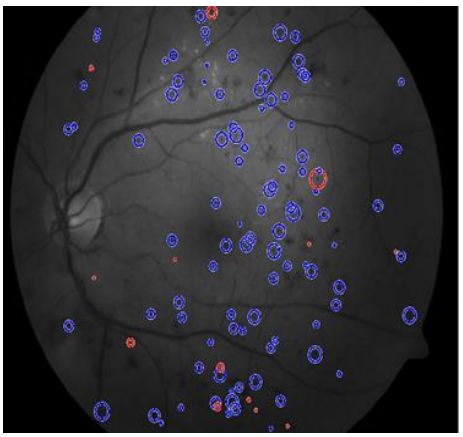

Figure 8. lesion level assessment(image021)

The lesion level evaluation of MA detection for one of the test images of e-ophtha and DIATRETDB1 database images is as shown in Figures 7 and 8 respectively, where blue circles indicate MAs lesions, i.e., True Positives, while red circles indicate Non-MAs, i.e., True Negatives as classified by the classifier. Then the obtained marked lesions are compared with the ground truth in order to get FP and FN. Then accuracy of the classifier is determined.

Three scales to measure the performance of the ensemble model for microaneurysm segmentation: accuracy (ACC), sensitivity (SEN), and specificity (SPE), which are based on true positive (TP), true negative (TN), false positive (FP), and false negative (FN), are employed. Tables 2 and 3 compare the proposed MA identification technique to current algorithms on the e-ophtha MA and DIARETDB1 databases, respectively.

Table 2. Comparison of performance metrics for the e-ophtha data set.

Author	Classifier	SEN	SPE	ACC	AUC
Long et al., 2020 [10]	Naive Bayes	-	-	82.1	0.81
Joshi & Karule, 2019 [18]	Mathematical Morphology	89.2	91	92.4	0.92
Smitha et al., 2018 [21]	ANN	90.6	80	88.09	0.89
Proposed	**Ensemble**	**90.7**	**90**	**93.2**	**0.928**

Table 3. Comparison of performance metrics for the DIARETDB1 data set.

Author	Classifier	SEN	SPE	ACC	AUC
Long et al., 2020 [10]	Naive Bayes	-	-	84.89	0.85
Shirbahadurkar [8]	FFNN	83	91	88	-
	SVM	77	88	84	-
Proposed	**Ensemble**	**85**	**91**	**87**	**0.87**

S. Long [10] suggested a directional local contrast feature, and 44 features were retrieved from the candidate patches in total. For MA and Non-MA classification, the collected features are given into the NB classifier. The patch-based categorization is carried out. In contrast, only 11 features were recovered in the suggested model, and the ensemble model was employed. For the Shirbahadurkar technique [8], significant computing time is needed to modify the neuron weights using a feed forward neural network, which has great specificity. When compared to approaches based on deep learning, the suggested method is simpler and faster since only optimum features are collected and a simple blood vessel segmentation method is performed. An ensemble method is described in [32], where model incorporates algorithms such as Random Forest, DT, Adaboost, KNN, and Logistic regression. The data in the set was first transformed, and all of the characteristics were supplied to the individual classifiers of the ensemble classifier, after which a voting technique was used to reach a conclusion. Our suggested technique is distinct in that it determines which classifier can make the best judgement over the rest of the ensemble model's classifiers based on the mean absolute difference of individual features, and the final decision is made based on a majority vote. Because [32] utilized a different data set, the findings could not be compared.

4. CONCLUSION

The proposed work provides a completely automated technique for MA detection in retinal fundus images, which may be utilized to diagnose the early stages of Diabetic Retinopathy. Preprocessing, morphological processing for candidate extraction, feature extraction, and a new ensemble classifier are used to achieve the goal. A novel technique to ensemble classification that is based on individual feature categorization has been developed. KNN, SVM, NB, and DT are the major supervised learning algorithms employed in the ensemble model. Using two freely accessible databases, e-ophtha MA and DIARETDB1, the suggested technique has been tested. The proposed technique produced results with sensitivity of 90.7%, specificity of 90% and accuracy of 93.2% on the e-ophtha-MA dataset. Similarly, sensitivity of 85%, specificity of 91% and accuracy of 87% were obtained on the DIARETDB1 dataset. ROC curves demonstrate proposed technique produced better results in terms of identifying MAs compared to individual classifiers in terms of AUC. Future studies will focus on enhancing the efficacy of MA identification by implementing ensemble deep learning techniques in order to obtain better outcomes.

CONFLICTS OF INTEREST

In relation to the research, writing, and/or publishing of this paper, the authors disclosed no possible conflicts of interest.

AUTHOR CONTRIBUTIONS

Mohamed Jebran P contributed to the formulation of the proposed method, the experiments, and the writing of the original draft preparation. Shweta Gupta supervised in the conceptualization, the problem formulation, the conduction of the research process, and article preparation. Mohamed Jebran P and Shweta Gupta validated the results and revised the manuscript. All authors read and approved the final manuscript.

REFERENCES

[1] S. Wild, G. Roglic, A. Green, R. Sicree and H. King, "Global prevalence of diabetes: estimates for the year 2000 and projections for 2030," *Diabetes care,* vol. 27, pp. 1047–1053, 2004.

[2] P. P. Goh, M. A. Omar, A. F. Yusoff et al., "Diabetic eye screening in Malaysia: findings from the National Health and Morbidity Survey 2006," *Singapore medical journal,* vol. 51, pp. 631, 2010.

[3] E. M. Kohner, S. J. Aldington, I. M. Stratton, S. E. Manley, R. R. Holman, D. R. Matthews, R. C. Turner et al., "United Kingdom Prospective Diabetes Study, 30: diabetic retinopathy at diagnosis of non–insulin-dependent diabetes mellitus and associated risk factors," *Archives of Ophthalmology,* vol. 116, pp. 297–303, 1998.

[4] R. Taylor and D. Batey, *Handbook of retinal screening in diabetes: diagnosis and management*, John Wiley & Sons, 2012.

[5] C. Suto, S. Hori, S. Kato, K. Muraoka and S. Kitano, "Effect of perioperative glycemic control in progression of diabetic retinopathy and maculopathy," *Archives of Ophthalmology,* vol. 124, pp. 38–45, 2006.

[6] D. A. Salz and A. J. Witkin, "Imaging in diabetic retinopathy," *Middle East African journal of ophthalmology,* vol. 22, pp. 145, 2015.

[7] S. Gupta, "Smartphone based Early Detection of Epileptic Seizures Using Machine Learning," *2020 12th International Conference on Bioinformatics and Biomedical Technology,* pp.38-42, 2020.

[8] S. D. Shirbahadurkar, V. M. Mane and D. V. Jadhav, "Early stage detection of diabetic retinopathy using an optimal feature set," 2017 *International Symposium on Signal Processing and Intelligent Recognition Systems*, pp.15-23, 2017.

[9] D. J. Derwin, S. T. Selvi, O. J. Singh and B. P. Shan, "A novel automated system of discriminating Microaneurysms in fundus images," *Biomedical Signal Processing and Control,* vol. 58, pp. 101839, 2020.

[10] S. Long, J. Chen, A. Hu, H. Liu, Z. Chen and D. Zheng, "Microaneurysms detection in color fundus images using machine learning based on directional local contrast," *Biomedical engineering online,* vol. 19, pp. 1–23, 2020.

[11] B. Wu, W. Zhu, F. Shi, S. Zhu and X. Chen, "Automatic detection of microaneurysms in retinal fundus images," *Computerized Medical Imaging and Graphics,* vol. 55, pp. 106–112, 2017.

[12] S. Wang, H. L. Tang, Y. Hu, S. Sanei, G. M. Saleh, T. Peto et al., "Localizing microaneurysms in fundus images through singular spectrum analysis," *IEEE Transactions on Biomedical Engineering,* vol. 64, pp. 990–1002, 2016.

[13] I. Lazar and A. Hajdu, "Retinal microaneurysm detection through local rotating cross-section profile analysis," *IEEE transactions on medical imaging,* vol. 32, pp. 400–407, 2012.

[14] L. Seoud, T. Hurtut, J. Chelbi, F. Cheriet and J. P. Langlois, "Red lesion detection using dynamic shape features for diabetic retinopathy screening," *IEEE transactions on medical imaging,* vol. 35, pp. 1116–1126, 2015.

[15] B. Antal and A. Hajdu, "An ensemble-based system for microaneurysm detection and diabetic retinopathy grading," *IEEE transactions on biomedical engineering,* vol. 59, pp. 1720–1726, 2012.

[16] A. Manjaramkar and M. Kokare, "Statistical geometrical features for microaneurysm detection," *Journal of digital imaging,* vol. 31, pp. 224–234, 2018.

[17] V. Dharani and R. Lavanya, "Improved microaneurysm detection in fundus images for diagnosis of diabetic retinopathy," 2017 *International Symposium on Signal Processing and Intelligent Recognition Systems*, pp.185-198, 2017.

[18] S. Joshi and P. T. Karule, "Mathematical morphology for microaneurysm detection in fundus images," *European journal of ophthalmology,* vol. 30, pp. 1135–1142, 2020.

[19] P. Chudzik, S. Majumdar, F. Calivá, B. Al-Diri and A. Hunter, "Microaneurysm detection using fully convolutional neural networks," *Computer methods and programs in biomedicine*, vol. 158, pp. 185–192, 2018.

[20] C. Lam, D. Yi, M. Guo and T. Lindsey, "Automated detection of diabetic retinopathy using deep learning," *AMIA summits on translational science proceedings,* vol. 2018, pp. 147, 2018.

[21] M. Smitha, A. K. Nisa and K. Archana, "Diabetic retinopathy detection in fundus image using cross sectional profiles and ann," *Computational Vision and Bio Inspired Computing*, Springer, pp. 982–993, 2018.

[22] E. Decenciere, G. Cazuguel, X. Zhang, G. Thibault, J.-C. Klein, F. Meyer, B. Marcotegui, G. Quellec, M. Lamard, R. Danno et al., "TeleOphta: Machine learning and image processing methods for teleophthalmology," *Irbm,* vol. 34, pp. 196–203, 2013.

[23] T. Kauppi, V. Kalesnykiene, J.-K. Kamarainen, L. Lensu, I. Sorri, A. Raninen, R. Voutilainen, H. Uusitalo, H. Kälviäinen and J. Pietilä, "The diaretdb1 diabetic retinopathy database and evaluation protocol.," em *BMVC,* vol.1,pp.1-10, 2007.

[24] K. Zuiderveld, "Contrast limited adaptive histogram equalization," em *Graphics gems IV,* pp. 474–485,1994.

[25] M. M. Habib, R. A. Welikala, A. Hoppe, C. G. Owen, A. R. Rudnicka and S. A. Barman, "Detection of microaneurysms in retinal images using an ensemble classifier," *Informatics in Medicine Unlocked,* vol. 9, pp. 44–57, 2017.

[26] A. D. Fleming, S. Philip, K. A. Goatman, J. A. Olson and P. F. Sharp, "Automated microaneurysm detection using local contrast normalization and local vessel detection," *IEEE transactions on medical imaging,* vol. 25, pp. 1223–1232, 2006.

[27] R. M. Haralick, K. Shanmugam and I. Dinstein, "Textural Features for Image Classification," *IEEE Transactions on Systems, Man, and Cybernetics,* Vol. SMC-3, pp. 610-621, 1973.

[28] M. Hall-Beyer, "GLCM texture: A tutorial v. 3.0 March 2017," 2017.

[29] O. Credit, "Bootstrap-inspired techniques in computational intelligence," *IEEE SIGNAL PROCESSING MAGAZINE,* vol. 1053, 2007.

[30] D. Veiga, N. Martins, M. Ferreira and J. Monteiro, "Automatic microaneurysm detection using laws texture masks and support vector machines," *Computer Methods in Biomechanics and Biomedical Engineering: Imaging & Visualization,* vol. 6, pp. 405–416, 2018.

[31] R. Saha, A. R. Chowdhury and S. Banerjee, "Diabetic retinopathy related lesions detection and classification using machine learning technology," 2016 *International Conference on Artificial Intelligence and Soft Computing*, pp.734-745,2016.

[32] G. T. Reddy, S. Bhattacharya, S. S. Ramakrishnan, C. L. Chowdhary, S. Hakak, R. Kaluri e M. P. K. Reddy, "An ensemble based machine learning model for diabetic retinopathy classification," *2020 International conference on emerging trends in information technology and engineering (ic-ETITE)*,pp.1-6, 2020.

BIOGRAPHY OF AUTHORS

Mohamed Jebran P received M. Tech degree in Electronics and Communication from DSCE, Bangalore, India, in 2010. He is currently pursuing the Ph.D. degree in the Faculty of Engineering and Technology, Jain University, Bangalore, India. He is also working as an Assistant Professor in Department of Electronics and Communication, HKBK College of Engineering. His research interest includes biomedical image processing, image processing and machine learning.

Dr. Shweta Gupta is Ph.D. in Electronics and Communication from Dr. K. N. Modi University, Rajasthan, India. M.S from Bits Pilani and B.E from Pune University and Executive M.B.A from I.I.M, Lucknow. She is all INDIA topper of C.B.S.E Board in 1997. Her research areas are Biomedical electronics with specialization in Epilepsy and Parkinson's disease. She is currently working as Associate Professor in Faculty of Engineering and Technology, Jain University, Bangalore, India. She was awarded by DST-SERB, Govt. of India as senior Scientist to present her research paper in Singapore in ICBBT 2015.